PHYSICAL REVIEW D **83,** 074509 (2011)

Running coupling constant of ten-flavor QCD with the Schrödinger functional method

M. Hayakawa,[1] K.-I. Ishikawa,[2] Y. Osaki,[2] S. Takeda,[3] S. Uno,[1] and N. Yamada[4,5,*]

[1]*Department of Physics, Nagoya University, Nagoya 464-8602, Japan*

[2]*Department of Physics, Hiroshima University, Higashi-Hiroshima 739-8526, Japan*

[3]*School of Mathematics and Physics, College of Science and Engineering, Kanazawa University, Kakuma-machi, Kanazawa, Ishikawa 920-1192, Japan*

[4]*KEK Theory Center, Institute of Particle and Nuclear Studies, High Energy Accelerator Research Organization (KEK), Tsukuba 305-0801, Japan*

[5]*School of High Energy Accelerator Science, The Graduate University for Advanced Studies (Sokendai), Tsukuba 305-0801, Japan*

(Received 11 November 2010; published 26 April 2011)

The walking technicolor theory attempts to realize electroweak symmetry breaking as the spontaneous chiral symmetry breakdown caused by the gauge dynamics with slowly varying gauge coupling constant and large mass anomalous dimension. Many-flavor QCD theories are candidates owning these features. We focus on the SU(3) gauge theory with ten flavors of massless fermions in the fundamental representation, and compute the gauge coupling constant in the Schrödinger functional scheme. Numerical simulation is performed with $O(a)$-unimproved lattice action, and the continuum limit is taken in linear in lattice spacing. We observe evidence that this theory possesses an infrared fixed point.

DOI: 10.1103/PhysRevD.83.074509 PACS numbers: 11.15.Ha

I. INTRODUCTION

While the standard model has been established through a number of experiments, unnatural hierarchies are present between the electroweak scale and the Planck scale and also among the fermion masses. The Large Hadron Collider (LHC) is expected to give new insight into these hierarchies. Among various new physics models proposed so far, the technicolor (TC) model [1] is one of the most attractive ones in these regards, as it does not require elementary scalar particles, which make the former hierarchy unnatural, and its extension, extended TC model [2], has a possibility to generate the Yukawa hierarchy in a dynamical way. For recent review articles, see, for example, Ref. [3].

TC should be a strongly coupled vectorlike gauge system, which triggers spontaneous chiral symmetry breaking (SχSB). It is widely known, however, that the simplest TC models obtained by rescaling ordinary QCD have already been ruled out by the S parameter [4] and flavor-changing neutral-current (FCNC) [5] constraints. Reference [6] suggests a series of TC models to circumvent the FCNC problem. Those TC models appeal to the gauge dynamics in which the effective gauge coupling constant runs slowly (i.e. ''walks'') at a relatively large value over a wide range of energy scale above the SχSB scale, and in which the chiral condensate gets large anomalous dimension. Such TC is called walking TC (WTC), and possible candidates have been enumerated through semiquantitative analyses [7]. Since the dynamics that underlie WTC significantly differ from those of two- or three-flavor QCD, the naive scaling argument in N_c or N_f to estimate the S parameter would not work, and any quantitative predictions from WTC require solving nonperturbative dynamics explicitly. Lattice gauge theory provides a unique way to study this class of models from the first principles at present.

The search for candidate theories of WTC is frequently linked to the N_f-dependent phase structure of the gauge theories. Let us take SU(3) gauge theory with N_f flavors of fermions in the fundamental representation as an example. According to the analysis of the perturbative β function, the system with large enough N_f ($N_f > 16.5$) is asymptotically nonfree and trivial unless a nontrivial ultraviolet fixed point exists. On the other hand, if N_f is sufficiently small ($N_f \leq 3$) the dynamics is QCD-like and thus in the chirally broken phase. It is believed that for the in-between N_f there exists a so-called conformal phase, where the coupling constant reaches an infrared fixed point (IRFP) without SχSB set in, but confinement may take place [8]. The range of N_f in which the conformal phase is realized is called conformal window, and is represented by $N_f^{\mathrm{crit}} < N_f < 16.5$. It is then natural to speculate that the gauge dynamics slightly below N_f^{crit} exhibit the features required for WTC; slow running of the gauge coupling constant and SχSB. The first goal in the search for WTC is thus to identify N_f^{crit}.

In the past years, many groups have used techniques of lattice simulations to search for N_f^{crit} and/or WTC through hadron spectrum, eigenvalue distribution of Dirac operator, the behavior of running coupling constant, or renormalization group analysis of candidate theories [9]. For nonlattice

*norikazu.yamada@kek.jp

studies, see, for example, Refs. [10,11]. Among various candidates, many-flavor QCD [12–19], sextet QCD [20–25], and two-color adjoint QCD [26–31] have been intensively studied. In this work, we focus on many-flavor QCD with $N_c = 3$ and fermions in the fundamental representation. In a seminal work [12], the running coupling constants were calculated for eight- and 12-flavor QCD using the Schrödinger functional (SF) scheme on the lattice [32]. They concluded that 12-flavor QCD has an IRFP at $g^2_{\rm SF} \sim 5$ while eight-flavor QCD does not. In practice, the study of the running coupling alone is supposed to be unable to fully exclude the possibility of a large IRFP because it requires lattice simulations at arbitrarily large coupling. Even worse, the unphysical, bulk first-order phase transition was found to occur in the strong coupling regime of several gauge theories [23,33,34]. In such simulations, there exists an upper limit on the bare coupling at which lattice calculation is sensible. Nevertheless, because of the supports from the spectroscopy studies [14,16,18], the conclusion in Ref. [12] that the eight-flavor QCD is QCD-like, i.e. $N_f^{\rm crit} > 8$, seems to be established nowadays.

After the work of Ref. [12], one group [15] has presented evidence of the conformality of 12-flavor QCD. The opposite conclusion, however, has also been reported by the other groups [16,18]. Therefore $N_f^{\rm crit} < 12$ is still under debate. Clearly, the observed contradiction must be clarified before going further. While in the spectroscopy study of 12-flavor QCD many sources of systematic uncertainties due to finite volume, taste breaking, chiral extrapolation, lack of continuum limit, etc. remain to be quantified, the calculation of the SF coupling constant of Ref. [12] appears, at present, to be less ambiguous. In such a circumstance, we are tempted to explore the dynamics of ten-flavor QCD. In this paper, we investigate, as a first step, the running coupling constant of ten-flavor QCD on the lattice to see whether it shows conformal behavior. We find that the running slows down and observe evidence that this theory possesses an infrared fixed point.

The paper is organized as follows. In Sec. II, we give remarks on how we identify IRFP on the lattice. Section III summarizes the coefficients relevant to the perturbative calculation of the running coupling constant for later use. In Sec. IV, the simulation setup including the definition of the running coupling constant in the Schrödinger functional scheme is presented. In Sec. V, we describe the analysis method and present the numerical results. Section VI is devoted to the summary and outlook.

II. REMARKS ON SEARCHING FOR IRFP ON THE LATTICE

Since there exists a subtlety in proving the existence of IRFP with lattice gauge theory, in this section we briefly explain what is actually calculated and then give how to identify the existence of IRFP. Here we focus on the concept only. For further details of the calculational and analysis method that we take, see the following sections.

In this work, we calculate the renormalized coupling constant in the Schrödinger functional scheme at two different length scales, L and $s \cdot L$. In practice, this is realized by repeating the calculation on two different volumes, l^4 and $(s \cdot l)^4$, at a common lattice bare coupling g_0^2, where $l = L/a$. We denote those couplings by u [or $g^2(g_0^2, l)$] and $g^2(g_0^2, s \cdot l)$, respectively. Using those, we define the discrete beta function (DBF) by $B(u, s, l) = 1/g^2(g_0^2, s \cdot l) - 1/u$, where the rescaling factor s is arbitrary but is fixed to 2. If the DBF is free from lattice discretization errors, the sign of this quantity may directly tell whether the coupling constant increases or decreases against the scale change by s at the scale L, which is implicitly set by the value of u that we can choose. Since discretization errors do exist, however, we need to take the continuum limit. The $a \to 0$ limit is taken for a fixed L, i.e. for a fixed u, by varying lattice spacing a. A series of the DBF thus obtained is then a function of l, and the $l = L/a \to \infty$ limit is expected to give the continuum limit. In summary, the DBF is constructed from a pair of lattice volumes $[l^4, (s \cdot l)^4]$, and choice of larger l results in the DBF closer to the continuum limit.

In practice, lattice spacing is varied by changing the lattice bare coupling g_0^2. If $g^2(g_0^2, l_2)$ turns out to be always larger than $g^2(g_0^2, l_1)$ with $l_2 > l_1$, $B(u, s, l) < 0$ should hold for any l and $s > 1$. In this case, the bare coupling at which $g^2(g_0^2, l_1)$ is equal to a fixed value u becomes small as lattice size l_1 increases or one approaches the continuum limit. Thus, the $a \to 0$ limit is realized in the $g_0^2 \to 0$ limit. This is the case for asymptotically free theories with no IRFP such as ordinary QCD, and no subtlety is present. Even if an IRFP exists in such theories, the situation does not change as long as the input u is smaller than the IRFP, $g^2_{\rm IRFP}$. In other words, if the DBF extrapolated to $l \to \infty$ (or equivalently $1/l \to 0$) is negative, the limiting value is interpreted as the continuum limit and the possibility that an IRFP exists below u is excluded.

When the DBF extrapolated to $l \to \infty$ is positive, interpretation of numerical results becomes ambiguous. In this case, in the vicinity of $1/l = 0$, $g^2(g_0^2, s \cdot l) < g^2(g_0^2, l)$, i.e. $B(u, s, l) > 0$. Indeed, it happens below $\beta = 4.4$ in Fig. 4 of Ref. [13], for example. Then, one may expect that the $l \to \infty$ limit is realized by $g_0^2 \to \infty$ on first sight. However, recalling ϕ^4 theory, this expectation turns out to be too naive. In ϕ^4 theory, the continuum limit exists only in the trivial case unless the theory possesses a nontrivial UV fixed point. Since the situation is similar to this case, the most plausible interpretation is that, when $u > g^2_{\rm IRFP}$, the continuum limit does not exist unless a nontrivial UV fixed point exists. Since no nontrivial UV fixed point has been established so far, it is not suitable to call the extrapolated value the continuum limit when it is positive. Nevertheless,

TABLE I. The perturbative IRFP obtained from the two-loop universal and the three-loop SF scheme analyses.

N_f	4	6	8	10	12	14	16
Two-loop universal				27.74	9.47	3.49	0.52
Three-loop SF with $\theta = \pi/5$	43.36	23.75	15.52	9.45	5.18	2.43	0.47

we can still infer that $u > g^2_{\rm IRFP}$ because no other possibility remains.

We investigate the sign of the DBF, starting with the weak coupling regime $u \sim 1$ where the perturbative calculation is reliable and predicts a negative value. We keep monitoring the sign of the DBF with increasing u. The identification of the IRFP is then made by sign flip of the DBF extrapolated to $l \to \infty$. Notice that, when the extrapolated value is positive, the extrapolation does not make sense and hence we do not insist that the continuum limit is determined.

III. PERTURBATIVE ANALYSIS

We start with defining the β function of an effective gauge coupling constant in a mass-independent renormalization scheme, which should have the following expansion in the perturbative regime,

$$\begin{aligned}\beta(g^2(L)) &= L\frac{\partial g^2(L)}{\partial L} \\ &= b_1 g^4(L) + b_2 g^6(L) + b_3 g^8(L) \\ &\quad + b_4 g^{10}(L) + \cdots,\end{aligned} \tag{1}$$

where L denotes a length scale. The first two coefficients on the right-hand side are scheme independent, and given by

$$\begin{aligned}b_1 &= \frac{2}{(4\pi)^2}\left[11 - \frac{2}{3}N_f\right], \\ b_2 &= \frac{2}{(4\pi)^4}\left[102 - \frac{38}{3}N_f\right].\end{aligned} \tag{2}$$

The remaining coefficients are scheme dependent and known only in the limited schemes and orders. The third coefficient takes the following form in the Schrödinger functional scheme:

$$b_3^{\rm SF} = b_3^{\overline{\rm MS}} + \frac{b_2 c_2^\theta}{2\pi} - \frac{b_1(c_3^\theta - c_2^{\theta 2})}{8\pi^2}, \tag{3}$$

where $b_3^{\overline{\rm MS}}$ is a coefficient in the $\overline{\rm MS}$ scheme,

$$b_3^{\overline{\rm MS}} = \frac{2}{(4\pi)^6}\left[\frac{2857}{2} - \frac{5033}{18}N_f + \frac{325}{54}N_f^2\right], \tag{4}$$

and the calculable quantities c_2^θ and c_3^θ depend on the spatial boundary condition imposed on the fermion fields in the SF setup, i.e. so-called θ. Those for $\theta = \pi/5$ and c_2^θ for $\theta = 0$ are known to be [35]

$$c_2^{\theta=\pi/5} = 1.255\,63 + 0.039\,863 \times N_f, \tag{5}$$

$$\begin{aligned}c_3^{\theta=\pi/5} &= (c_2^{\theta=\pi/5})^2 + 1.197(10) + 0.140(6) \times N_f \\ &\quad - 0.0330(2) \times N_f^2,\end{aligned} \tag{6}$$

$$c_2^{\theta=0} = 1.255\,63 + 0.022\,504 \times N_f, \tag{7}$$

but $c_3^{\theta=0}$ has not been calculated yet. Although $\theta = 0$ is chosen in our simulation as described in Sec. IV, the coefficients for $\theta = \pi/5$ are used only to see the situation of conformal windows inferred just from the perturbative analysis, and the potential size of difference between the two- and three-loop calculations.

The perturbative estimates of the infrared fixed point (IRFP) for SU(3) gauge theory with N_f flavors of fundamental fermion are summarized in Table I. We note that in the three-loop perturbative analysis the existence of IRFP is determined only by the sign of b_3, which is always negative for the range of N_f shown in Table I. Therefore, the existence of IRFP as well as its value may be unstable against including higher orders. Nevertheless, for $N_f \geq 14$ the difference between the two- and three-loop results is reasonably small, and one may expect that higher order corrections do not spoil the existence of IRFP or even do not change its value by much for such a large N_f.

According to the analysis based on the Schwinger-Dyson equation, SχSB is expected to occur when the running coupling constant reaches $g^2 \sim \pi^2$ in SU(3) gauge theories [36]. In spite of the scheme dependence of the running coupling constant and the value of IRFP, those results motivate us to speculate that ten-flavor QCD may exhibit strongly coupled walking dynamics, and thus deserves full nonperturbative calculation.

IV. SIMULATION DETAILS

A. Schrödinger functional

We employ the Schrödinger functional (SF) method [32] to study the scale dependence of the running coupling constant. Unimproved Wilson fermion action and the standard plaquette gauge action are used without any boundary counterterms as described below.

The SF on the lattice is defined on a four-dimensional hypercubic lattice with a volume $(L/a)^3 \times (T/a)$ in the cylindrical geometry. Throughout this work, the temporal extent T/a is chosen to be equal to the spatial one L/a. The

periodic boundary condition in the spatial directions with vanishing phase factor ($\theta = 0$) and the Dirichlet one in the temporal direction are imposed for both gauge [$U_\mu(x)$] and fermion [$\psi(x)$ and $\bar{\psi}(x)$] fields. The boundary values for gauge and fermion fields are represented by three-by-three color matrices, C and C', and spinors, ρ, ρ', $\bar{\rho}$, and $\bar{\rho}'$, respectively. The partition function of this system is given by

$$Z_{\mathrm{SF}}(C', \bar{\rho}', \rho'; C, \bar{\rho}, \rho) = e^{-\Gamma(C', \bar{\rho}', \rho'; C, \bar{\rho}, \rho)} = \int D[U, \psi, \bar{\psi}] e^{-S[U, \psi, \bar{\psi}, C, C', \rho, \rho', \bar{\rho}, \bar{\rho}']}, \tag{8}$$

where Γ is the effective action, and

$$S[U, \psi, \bar{\psi}, C, C', \rho, \rho', \bar{\rho}, \bar{\rho}'] = S_g[U, C, C'] + S_q[U, \psi, \bar{\psi}, \rho, \rho', \bar{\rho}, \bar{\rho}']. \tag{9}$$

For the pure gauge part, we employ the plaquette action,

$$S_g[U, C, C'] = \frac{\beta}{6} \sum_x \sum_{\mu=0}^{3} \sum_{\nu=0}^{3} \bar{\delta}_{\mu,\nu} w_{\mu,\nu}(x_0) \times \mathrm{Tr}[1 - P_{\mu,\nu}(x)], \tag{10}$$

where $\beta = 6/g_0^2$ denotes the inverse of the bare coupling constant, $\bar{\delta}_{\mu,\nu} = 0$ when $\mu = \nu$ otherwise 1, and $P_{\mu,\nu}(x)$ denotes a 1×1 Wilson loop on the μ-ν plane starting and ending at x. The spatial link variables on the boundaries, the hypersurfaces at $x_0 = 0$, and L/a, are all set to the diagonal, constant $SU(3)$ matrices as

$$U_k(x)|_{x_0=0} = \exp[C], \qquad C = \frac{ia}{L} \begin{pmatrix} \eta - \frac{\pi}{3} & 0 & 0 \\ 0 & -\frac{1}{2}\eta & 0 \\ 0 & 0 & -\frac{1}{2}\eta + \frac{\pi}{3} \end{pmatrix}, \tag{11}$$

$$U_k(x)|_{x_0=L/a} = \exp[C'], \qquad C' = \frac{ia}{L} \begin{pmatrix} -\eta - \pi & 0 & 0 \\ 0 & \frac{1}{2}\eta + \frac{\pi}{3} & 0 \\ 0 & 0 & \frac{1}{2}\eta + \frac{2\pi}{3} \end{pmatrix}, \tag{12}$$

where $k = 1, 2, 3$, and η is parametrizing the gauge boundary fields. The weight $w_{\mu,\nu}(x_0)$ in Eq. (10) is given by

$$w_{\mu,\nu}(x_0) = \begin{cases} c_t & \text{for } (t = 0 \text{ or } t = (L/a) - 1) \text{ and } (\mu \text{ or } \nu = 0) \\ 0 & \text{for } (t = (L/a)) \text{ and } (\mu \text{ or } \nu = 0) \\ \frac{1}{2} c_s & \text{for } (t = 0 \text{ or } t = (L/a)) \text{ and } (\mu \neq 0 \text{ and } \nu \neq 0) \\ 1 & \text{for all the other cases.} \end{cases} \tag{13}$$

By tuning c_t, $O(a)$ errors induced from the boundaries in the time direction can be removed perturbatively, but in this work we simply take its tree level values, $c_t = 1$. With this setup, the value of c_s can be arbitrarily chosen because the spatial plaquettes on the boundaries do not contribute to the action. We thus set $c_s = 0$.

The fermion fields are described by the unimproved Wilson fermion action,

$$S_q[U, \psi, \bar{\psi}] = N_f \sum_{x,y} \bar{\psi}(x) D(x, y; U) \psi(y) = N_f \sum_{x,y} \bar{\psi}^{\mathrm{lat}}(x) D^{\mathrm{lat}}(x, y; U) \psi^{\mathrm{lat}}(y), \tag{14}$$

$$D^{\mathrm{lat}}(x, y; U) = \delta_{xy} - \kappa \sum_\mu \{(1 - \gamma_\mu) U_\mu(x) \delta_{x+\hat{\mu},y} + (1 + \gamma_\mu) U_\mu^\dagger(x - \hat{\mu}) \delta_{x-\hat{\mu},y}\}, \tag{15}$$

where

$$\psi^{\mathrm{lat}}(x) = \frac{1}{\sqrt{2\kappa}} \psi(x), \qquad \bar{\psi}^{\mathrm{lat}}(x) = \frac{1}{\sqrt{2\kappa}} \bar{\psi}(x), \qquad D^{\mathrm{lat}}(x, y; U) = 2\kappa D(x, y; U). \tag{16}$$

The hopping parameter κ is related to the bare mass m_0 through $2\kappa = 1/(am_0 + 4)$. The dynamical degrees of freedom of the fermion field $\psi(x)$ and antifermion fields $\bar{\psi}(x)$ reside on the lattice sites x with $0 < x_0 < T$. On both boundaries ($x_0 = 0$ and T), the half of the Dirac components are set to zero and the remaining components are fixed to some prescribed values, ρ, $\bar{\rho}$, ρ', and $\bar{\rho}'$, as

$$P_+ \psi(x)|_{x_0=0} = \rho(\mathbf{x}), \qquad P_- \psi(x)|_{x_0=0} = 0, \tag{17}$$

$$P_- \psi(x)|_{x_0=T} = \rho'(\mathbf{x}), \qquad P_+ \psi(x)|_{x_0=T} = 0, \tag{18}$$

$$\bar{\psi}(x) P_-|_{x_0=0} = \bar{\rho}(\mathbf{x}), \qquad \bar{\psi}(x) P_+|_{x_0=0} = 0, \tag{19}$$

$$\bar{\psi}(x) P_+|_{x_0=T} = \bar{\rho}'(\mathbf{x}), \qquad \bar{\psi}(x) P_-|_{x_0=T} = 0, \tag{20}$$

where $P_\pm = (1 \pm \gamma_0)/2$. In this work, the boundary values for the fermion fields are set to zero, i.e.,

$$\rho = \rho' = \bar{\rho} = \bar{\rho}' = 0. \tag{21}$$

B. Definition of the running coupling

With the gauge boundary conditions (11) and (12), the absolute minimum of the action is given by a color-electric background field denoted by $B(x)$. Then, the effective action can be defined as a function of B by

$$\Gamma[B] = -\ln Z_{\mathrm{SF}}(C', \bar{\rho}', \rho'; C, \bar{\rho}, \rho), \tag{22}$$

which has the following perturbative expansion in the bare coupling constant,

$$\Gamma = \frac{1}{g_0^2}\Gamma_0 + \Gamma_1 + O(g_0^2), \tag{23}$$

and, in particular, the lowest-order term,

$$\Gamma_0 = [g_0^2 S_g[B]]_{g_0=0}, \tag{24}$$

is exactly the classical action of the induced background field. The SF scheme coupling is then defined in the massless limit for fermions by

$$\left.\frac{\partial\Gamma}{\partial\eta}\right|_{\eta=0} = \frac{1}{g_{\mathrm{SF}}^2(g_0^2, l = L/a)} \left.\frac{\partial\Gamma_0}{\partial\eta}\right|_{\eta=0} = \frac{k}{g_{\mathrm{SF}}^2(g_0^2, l)}, \tag{25}$$

where the normalization constant k is determined such that $g_{\mathrm{SF}}^2 = g_0^2$ holds in the leading order of the perturbative expansion, and is found to be

$$k = \left.\frac{\partial\Gamma_0}{\partial\eta}\right|_{\eta=0} = 12\left(\frac{L}{a}\right)^2[\sin(2\gamma) + \sin(\gamma)] = k \quad \text{with } \gamma = \frac{\pi}{3}\left(\frac{a}{L}\right)^2. \tag{26}$$

Because of the absence of the clover term, only the η derivative of the gauge action contributes to $1/g_{\mathrm{SF}}^2(g_0^2, l)$.

C. Parameters

The simulation was performed on the lattice sizes of $l^4 = (L/a)^4 = 4^4$, 6^4, 8^4, 12^4, and 16^4 with the inverse of bare gauge coupling constant $\beta = 6/g_0^2$ in the range, $4.4 \leq \beta \leq 96.0$. However, the data from $l = 4$ lattices are not used in the following analysis because it was found that they have large discretization errors. We calculated the SF coupling on 18^4 lattice with a single β ($\beta = 4.55$), and the result is used to check the scaling violation at a specific value of g_{SF}^2.

The algorithm to generate the gauge configuration follows the standard hybrid Monte Carlo (HMC) with five

TABLE II. Simulation parameters and results obtained at $L/a = 6$.

β	κ	Trajectories	Plaquette	$\delta\tau$	Acceptance	g_{SF}^2	M
96.0000	0.126 703 0	39 700	0.979 268(0.000 002)	0.0076	0.827(0.002)	0.064 31(0.000 06)	0.000 12(0.000 03)
96.0000	0.126 707 0	49 900	0.979 267(0.000 002)	0.0076	0.826(0.002)	0.064 28(0.000 05)	−0.000 04(0.000 03)
48.0000	0.127 606 0	40 100	0.958 852(0.000 005)	0.0098	0.857(0.002)	0.132 21(0.000 10)	−0.000 13(0.000 02)
48.0000	0.127 610 0	41 100	0.958 846(0.000 004)	0.0098	0.857(0.002)	0.132 09(0.000 10)	−0.000 16(0.000 02)
24.0000	0.129 518 0	24 700	0.917 566(0.000 009)	0.0149	0.848(0.002)	0.280 79(0.000 15)	0.000 06(0.000 02)
24.0000	0.129 520 0	60 300	0.917 562(0.000 005)	0.0152	0.838(0.002)	0.280 86(0.000 10)	0.000 06(0.000 01)
12.0000	0.133 964 0	48 700	0.833 056(0.000 014)	0.0250	0.812(0.002)	0.644 50(0.000 76)	−0.000 04(0.000 05)
9.6000	0.136 568 0	160 300	0.789 765(0.000 012)	0.0256	0.826(0.001)	0.871 89(0.000 68)	0.000 02(0.000 03)
7.4000	0.141 069 0	120 500	0.724 148(0.000 015)	0.0270	0.854(0.001)	1.304 13(0.001 94)	0.000 06(0.000 06)
6.8000	0.143 052 0	120 300	0.698 517(0.000 018)	0.0270	0.870(0.001)	1.510 24(0.002 44)	−0.000 25(0.000 08)
6.3000	0.145 140 0	17 400	0.673 231(0.000 076)	0.0333	0.817(0.001)	1.747 88(0.005 05)	0.000 15(0.000 19)
6.0000	0.146 638 0	33 600	0.655 993(0.000 034)	0.0333	0.837(0.002)	1.936 84(0.006 91)	0.000 44(0.000 21)
6.0000	0.146 641 0	80 300	0.655 981(0.000 029)	0.0333	0.833(0.001)	1.936 05(0.003 62)	0.000 04(0.000 10)
5.5000	0.149 759 0	50 300	0.622 923(0.000 025)	0.0370	0.817(0.002)	2.383 40(0.010 92)	0.000 42(0.000 20)
5.5000	0.149 761 0	36 000	0.622 942(0.000 027)	0.0357	0.827(0.002)	2.362 32(0.006 34)	−0.000 18(0.000 22)
5.5000	0.149 762 0	140 300	0.622 977(0.000 023)	0.0357	0.831(0.001)	2.375 42(0.009 63)	0.000 23(0.000 14)
5.2000	0.152 133 0	220 300	0.600 097(0.000 019)	0.0380	0.812(0.001)	2.806 68(0.012 46)	−0.000 15(0.000 14)
5.0000	0.153 980 0	59 900	0.583 463(0.000 049)	0.0400	0.806(0.002)	3.288 37(0.066 18)	−0.000 05(0.000 46)
4.6000	0.158 514 0	33 800	0.545 776(0.000 055)	0.0400	0.813(0.002)	5.470 08(0.130 64)	0.000 92(0.000 43)
4.6000	0.158 515 0	150 000	0.545 680(0.000 041)	0.0400	0.813(0.001)	5.412 63(0.098 91)	0.001 23(0.000 42)
4.5000	0.159 902 0	100 300	0.535 280(0.000 061)	0.0400	0.813(0.001)	7.025 16(0.244 79)	0.001 11(0.000 69)
4.5000	0.159 903 0	100 300	0.535 305(0.000 066)	0.0400	0.813(0.002)	6.705 75(0.196 22)	0.000 33(0.000 61)
4.4215	0.161 068 0	105 900	0.526 537(0.000 087)	0.0385	0.825(0.001)	8.888 82(0.369 44)	0.002 38(0.000 97)
4.4215	0.161 082 0	92 400	0.526 692(0.000 066)	0.0385	0.826(0.001)	8.901 39(0.323 55)	0.000 73(0.000 75)
4.4000	0.161 421 0	249 500	0.524 331(0.000 060)	0.0400	0.811(0.001)	9.601 63(0.196 61)	0.000 51(0.000 50)
4.4000	0.161 422 0	182 500	0.524 342(0.000 091)	0.0400	0.812(0.001)	10.179 80(0.339 90)	0.001 19(0.000 73)
4.4000	0.161 423 0	250 500	0.524 387(0.000 062)	0.0400	0.811(0.001)	10.077 13(0.253 79)	0.000 49(0.000 53)

TABLE III. Simulation parameters and results obtained at $L/a = 8$.

β	κ	Trajectories	Plaquette	$\delta\tau$	Acceptance	g^2_{SF}	M
96.0000	0.126 327 0	22 500	0.979 420(0.000 002)	0.0056	0.811(0.004)	0.064 34(0.000 04)	0.000 01(0.000 01)
48.0000	0.127 225 0	18 300	0.958 843(0.000 003)	0.0100	0.818(0.007)	0.132 47(0.000 17)	0.000 02(0.000 02)
24.0000	0.129 145 0	42 300	0.917 260(0.000 004)	0.0125	0.804(0.003)	0.282 82(0.000 23)	−0.000 04(0.000 02)
12.0000	0.133 585 0	68 500	0.832 266(0.000 007)	0.0167	0.828(0.005)	0.653 80(0.000 71)	−0.000 10(0.000 03)
9.6000	0.136 180 0	21 820	0.788 830(0.000 013)	0.0200	0.828(0.006)	0.887 51(0.002 87)	−0.000 08(0.000 05)
7.4000	0.140 660 0	63 330	0.723 081(0.000 010)	0.0250	0.818(0.003)	1.341 82(0.004 17)	−0.000 04(0.000 16)
6.8000	0.142 620 0	41 500	0.697 409(0.000 013)	0.0250	0.797(0.002)	1.562 32(0.006 62)	0.000 12(0.000 11)
6.3000	0.144 700 0	28 000	0.672 208(0.000 021)	0.0250	0.816(0.003)	1.819 87(0.010 36)	−0.000 34(0.000 14)
6.0000	0.146 200 0	47 000	0.654 999(0.000 012)	0.0250	0.820(0.003)	2.012 48(0.012 58)	−0.000 42(0.000 11)
5.5000	0.149 270 0	35 900	0.622 016(0.000 021)	0.0286	0.797(0.003)	2.481 39(0.019 69)	−0.000 21(0.000 15)
5.0000	0.153 360 0	27 900	0.582 458(0.000 038)	0.0250	0.825(0.004)	3.469 30(0.072 38)	0.000 94(0.000 34)
4.8000	0.155 427 0	114 500	0.564 464(0.000 020)	0.0250	0.860(0.001)	4.353 48(0.098 45)	0.000 26(0.000 24)
4.7000	0.156 550 0	35 400	0.554 789(0.000 040)	0.0256	0.854(0.002)	4.875 95(0.210 35)	0.000 27(0.000 51)
4.6200	0.157 550 0	86 300	0.546 856(0.000 030)	0.0312	0.783(0.001)	6.237 44(0.25321)	−0.000 23(0.000 33)
4.6000	0.157 780 0	149 300	0.544 695(0.000 027)	0.0250	0.852(0.002)	6.011 08(0.170 93)	−0.000 07(0.000 28)
4.5500	0.158 420 0	24 500	0.539 428(0.000 090)	0.0278	0.833(0.003)	6.920 22(0.464 91)	0.000 87(0.000 88)
4.5500	0.158 427 0	93 300	0.539 336(0.000 033)	0.0278	0.831(0.002)	6.994 32(0.318 73)	0.001 35(0.000 41)
4.5500	0.158 450 0	25 700	0.539 683(0.000 064)	0.0278	0.832(0.004)	6.741 87(0.469 70)	−0.001 63(0.000 71)
4.5200	0.158 850 0	56 570	0.536 316(0.000 058)	0.0278	0.827(0.002)	8.280 29(0.576 87)	−0.000 10(0.000 59)
4.5000	0.159 130 0	107 100	0.534 108(0.000 036)	0.0250	0.859(0.001)	8.406 30(0.373 69)	−0.000 07(0.000 38)
4.4800	0.159 400 0	41 555	0.531 781(0.000 085)	0.0250	0.827(0.002)	8.572 14(0.572 02)	0.000 27(0.000 70)
4.4215	0.160 264 0	160 900	0.525 143(0.000 050)	0.0263	0.837(0.001)	12.218 77(0.496 25)	−0.000 12(0.000 41)
4.4215	0.160 270 0	127 500	0.525 149(0.000 058)	0.0250	0.861(0.001)	12.623 65(0.689 80)	−0.000 59(0.000 48)
4.4200	0.160 270 0	29 700	0.524 651(0.000 132)	0.0278	0.828(0.002)	13.150 85(0.997 74)	0.002 14(0.000 75)
4.4000	0.160 600 0	229 500	0.522 502(0.000 057)	0.0278	0.819(0.002)	15.007 64(0.691 15)	0.000 20(0.000 42)

pseudofermion fields introduced to simulate the ten flavors of dynamical fermions. The numerical simulations were carried out on several different architectures including general purpose graphics processing unit, PC cluster, and supercomputers. In order to achieve high performance on each architecture, the HMC code, especially the fermion solver part, was optimized depending on each architecture. In particular, mixed precision solver using multiple

TABLE IV. Simulation parameters and results obtained at $L/a = 12$.

β	κ	Trajectories	Plaquette	$\delta\tau$	Acceptance	g^2_{SF}	M
48.0000	0.126 970 0	11 200	0.958 648(0.000 002)	0.0056	0.815(0.003)	0.133 04(0.000 33)	−0.000 14(0.000 03)
24.0000	0.128 892 9	54 620	0.916 777(0.000 002)	0.0083	0.798(0.002)	0.284 32(0.000 36)	−0.000 08(0.000 02)
12.0000	0.133 335 9	68 955	0.831 306(0.000 003)	0.0125	0.808(0.002)	0.660 07(0.001 19)	−0.000 12(0.000 03)
9.6000	0.135 935 0	86 700	0.787 681(0.000 003)	0.0133	0.806(0.002)	0.903 25(0.002 33)	−0.000 01(0.000 03)
7.4000	0.140 406 0	106 050	0.721 824(0.000 004)	0.0154	0.795(0.004)	1.368 96(0.005 43)	−0.000 01(0.000 04)
6.8000	0.142 325 0	45 150	0.696 157(0.000 006)	0.0167	0.819(0.002)	1.599 98(0.009 83)	0.000 91(0.000 06)
6.3000	0.144 405 0	23 500	0.671 015(0.000 014)	0.0182	0.767(0.002)	1.890 12(0.016 92)	0.000 13(0.000 12)
6.0000	0.145 900 0	43 296	0.653 900(0.000 008)	0.0182	0.820(0.007)	2.106 12(0.022 02)	0.000 11(0.000 07)
5.8000	0.147 020 0	43 400	0.641 479(0.000 007)	0.0182	0.799(0.002)	2.221 71(0.028 02)	−0.000 09(0.000 07)
5.5000	0.148 940 0	45 200	0.621 162(0.000 012)	0.0167	0.842(0.003)	2.589 33(0.024 96)	0.000 17(0.000 17)
5.2000	0.151 200 0	68 000	0.598 557(0.000 009)	0.0200	0.781(0.002)	3.062 12(0.032 10)	0.000 56(0.000 09)
5.0800	0.152 235 0	25 480	0.588 819(0.000 013)	0.0167	0.848(0.002)	3.39 969(0.089 24)	0.000 15(0.000 13)
5.0000	0.152 970 0	90 921	0.582 135(0.000 019)	0.0167	0.826(0.002)	3.673 56(0.089 08)	−0.000 44(0.000 20)
4.8000	0.154 970 0	194 300	0.564 213(0.000 006)	0.0182	0.810(0.002)	4.848 05(0.145 09)	0.000 09(0.000 11)
4.6000	0.157 230 0	127 922	0.544 423(0.000 012)	0.0182	0.818(0.002)	7.298 85(0.385 89)	0.0007 5(0.000 17)
4.5500	0.157 850 0	57 260	0.539 025(0.000 021)	0.0192	0.802(0.002)	10.152 31(1.118 27)	0.001 25(0.000 27)
4.5000	0.158 550 0	104 570	0.534 014(0.000 049)	0.0250	0.701(0.007)	13.039 15(1.339 94)	−0.002 37(0.000 39)

TABLE V. Simulation parameters and results obtained at $L/a = 16$.

β	κ	Trajectories	Plaquette	$\delta\tau$	Acceptance	$g^2_{\rm SF}$	M
24.0000	0.128 8000	22 890	0.916 505(0.000 002)	0.0067	0.796(0.003)	0.283 68(0.000 57)	0.000 11(0.000 02)
12.0000	0.133 259 0	40 950	0.830 799(0.000 003)	0.0091	0.718(0.011)	0.663 84(0.002 93)	−0.000 16(0.000 02)
9.6000	0.135 860 0	30 900	0.787 096(0.000 002)	0.0080	0.807(0.003)	0.905 38(0.005 70)	−0.000 23(0.000 03)
7.4000	0.140 325 0	62 300	0.721 190(0.000 003)	0.0111	0.812(0.002)	1.390 94(0.008 34)	−0.000 02(0.000 03)
6.8000	0.142 290 0	39 796	0.695 613(0.000 004)	0.0133	0.787(0.002)	1.635 62(0.016 49)	−0.000 42(0.000 05)
6.3000	0.144 340 0	69 000	0.670 503(0.000 004)	0.0133	0.798(0.002)	1.914 12(0.016 28)	−0.000 36(0.000 04)
6.0000	0.145 795 0	18 900	0.653 363(0.000 007)	0.0156	0.712(0.004)	2.121 47(0.038 87)	0.000 43(0.000 10)
5.5000	0.148 850 0	50 330	0.620 911(0.000 007)	0.0143	0.782(0.002)	2.679 36(0.038 97)	−0.000 47(0.000 11)
5.0800	0.152 131 0	23 760	0.588 803(0.000 007)	0.0139	0.804(0.003)	3.247 42(0.072 71)	−0.000 03(0.000 12)
5.0000	0.152 855 0	71 954	0.582 121(0.000 004)	0.0143	0.797(0.002)	3.867 09(0.126 22)	−0.000 04(0.000 09)
4.8000	0.154 831 0	46 000	0.564 445(0.000 008)	0.0156	0.755(0.002)	5.729 11(0.490 13)	0.000 03(0.000 14)
4.6000	0.157 050 0	83 705	0.544 764(0.000 008)	0.0143	0.794(0.001)	8.212 43(0.631 14)	0.001 28(0.000 12)
4.5500	0.157 675 0	107 069	0.539 609(0.000 010)	0.0139	0.809(0.002)	10.814 52(0.800 73)	0.000 11(0.000 11)
4.5200	0.158 065 0	42 400	0.536 387(0.000 021)	0.0156	0.754(0.002)	17.341 93(3.728 29)	−0.000 30(0.000 21)

TABLE VI. Simulation parameters and results obtained at $L/a = 18$.

β	κ	Trajectories	Plaquette	$\delta\tau$	Acceptance	$g^2_{\rm SF}$	M
4.5500	0.157 650 0	32 309	0.540 093(0.000 014)	0.0143	0.785(0.003)	11.131 31(1.413 81)	−0.001 24(0.000 18)

graphics processing units (GPUs) enables us to obtain high statistics on $g^2_{\rm SF}$ at $l^4 = 12^4$ and 16^4 [37]. The acceptance ratio is kept to around 80% by adjusting the molecular dynamics step size ($\delta\tau$).

Since the Wilson fermion explicitly breaks chiral symmetry, the value of κ is tuned, for every pair of $(\beta, L/a)$, to its critical value κ_c realizing the massless fermion by monitoring the mass defined through the partially conserved axial-vector current (PCAC) relation. The values of β, κ, the number of trajectories, $\delta\tau$ and the results for $l = L/a = 6, 8, 12, 16,$ and 18 lattices are tabulated in Tables II, III, IV, V, and VI, respectively.

D. Comment on $O(a)$ unimprovement

In our pilot study, we employed the $O(a)$-improved fermion action with the perturbatively determined counterterms. With this setup, we encountered a sudden change of the plaquette and the PCAC mass at $l = 6$ and $\beta = 3.6$ when κ was decreased from 0.1517, and we could not realize the vanishing PCAC mass. The expected SF coupling constant is about 3–4 there. The same phenomenon also occurs on $l = 4$ lattices at almost the same value of bare coupling constant. Since the observed behavior looks similar to those reported in Refs. [23,33,34], we infer that this is a bulk, first-order phase transition. In order to cover the region $g^2_{\rm SF} \sim O(10)$, we omitted any $O(a)$ improvements. Thus, the leading discretization error in our result is linear in lattice spacing.

Even without $O(a)$ improvements, the bulk, first-order phase transition is observed for $\beta = 6/g_0^2 \sim 4.4$. However, this time it happens at the renormalized coupling constant greater than the $O(a)$-improved case, typically $g^2_{\rm SF} \sim O(10)$. Since this bulk phase transition is considered as a lattice artifact, whenever this happens we discard the gauge configurations at such β. Thus, the position of the critical β (~ 4.4) sets the lower limit on our exploration of β.

V. ANALYSIS METHOD AND RESULTS

A. Raw data

The SF coupling constant ($g^2_{\rm SF}$) and the PCAC mass (M) obtained on each (β, κ, l) are shown in Tables II, III, IV, V, and VI. $g_0^2/g^2_{\rm SF}$ is plotted as a function of the bare coupling constant g_0^2 in Fig. 1. The figure shows that $g^2_{\rm SF}$ increases with $l = L/a$ at a fixed g_0^2, but the change between the data from $l = 12$ and $l = 16$ is tiny. For later use, we fit the data of $g_0^2/g^2_{\rm SF}$ to an interpolating formula as a function of the bare coupling constant g_0^2. Among various functional forms we examined, the following form,

$$\frac{g_0^2}{g^2_{\rm SF}(g_0^2, l)} = \frac{1 - a_{l,1} g_0^4}{1 + p_{1,l} \times g_0^2 + \sum_{n=2}^{N} a_{l,n} \times g_0^{2n}}, \qquad (27)$$

turned out to give the minimum χ^2/dof for a fixed number of free parameters, N. We thus employ Eq. (27). In Eq. (27), $p_{1,l}$ is the l-dependent coefficient and we have calculated them perturbatively in the SF scheme:

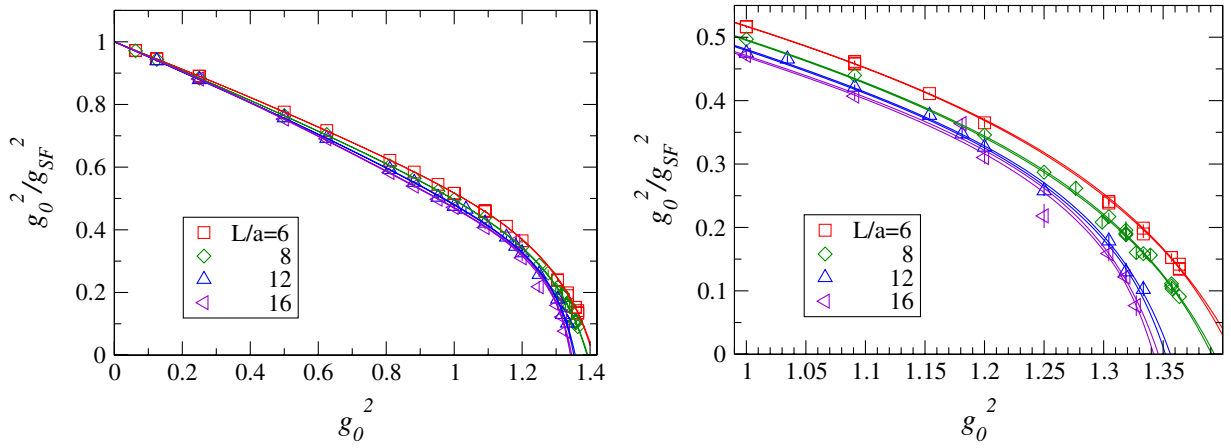

FIG. 1 (color online). g_0^2 dependence of $g_0^2/g_{\rm SF}^2$ for $l = L/a = 6$, 8, 12, and 16. The right panel magnifies the region of $g_0^2 \in [1.1, 1.40]$.

$$p_{1,l} = \begin{cases} 0.447\,710\,783\,1 & \text{for } l = 6 \\ 0.462\,481\,340\,8 & \text{for } l = 8 \\ 0.475\,688\,826\,0 & \text{for } l = 12 \\ 0.483\,307\,920\,3 & \text{for } l = 16 \\ 0.486\,476\,795\,8 & \text{for } l = 18. \end{cases} \tag{28}$$

The other coefficients $a_{l,n}$'s are determined for each l independently. We optimize the degree of polynomial N in the denominator of Eq. (27) by monitoring χ^2/dof, and take $N = 5$ for $l = 6$ and 12, and $N = 4$ for $l = 8$ and 16. Table VII shows the fit results for the coefficients in Eq. (27). The fit results are also shown as the region sandwiched by a pair of solid curves in Fig. 1.

Hereafter we denote the SF coupling obtained at a bare coupling constant g_0^2 and at a lattice length of l by $g_{\rm SF}^2(g_0^2, l)$ and its continuum counterpart by $g_{\rm SF}^2(L)$.

B. Discrete β function

In order to see the scale dependence of the SF coupling constant, we analyze the discrete β function (DBF) introduced in Refs. [20,23]. The whole procedure is described below.

First, we choose an initial value of the running coupling constant, denoted by u. This implicitly sets the initial length scale L_0 through $g_{\rm SF}^2(L_0) = u$. Using the interpolating formula (27) for the lattice size l ($= L/a$), the bare coupling constant g_0^* is numerically obtained by solving the equation $g_{\rm SF}^2(g_0^{*2}, l) = u$. l is identified with L_0/a, so that the lattice spacing at g_0^{*2} is found to be $a(g_0^{*2}, l) = L_0/l$. Now we choose a rescaling factor, s. The lattice step scaling function $\Sigma_0(u, s, l)$ is then defined as the SF coupling for $l' = s \cdot l$ at the same bare coupling g_0^{*2}, i.e.,

$$\Sigma_0(u, s, l) \equiv g_{\rm SF}^2(g_0^{*2}, s \cdot l)|_{g_{\rm SF}^2(g_0^{*2}, l) = u}. \tag{29}$$

The meaning of the subscript "0" becomes clear soon. Of course, both l and $s \cdot l$ must be equal to one of 6, 8, 12, and 16, and hence the possible values for the rescaling factor s are limited. The difference between $\Sigma_0(u, s, l)$ and u gives the scale dependence through the scale change from L to $s \cdot L$, up to lattice artifacts.

TABLE VII. The results for the coefficients in the fit function (27).

L/a	N	χ^2/dof	$a_{L/a,1}$	$a_{L/a,2}$	$a_{L/a,3}$	$a_{L/a,4}$	$a_{L/a,5}$
6	3	9.0(1.3)	0.4906(0.0025)	−0.2749(0.0105)	−0.1897(0.0151)		
6	4	1.4(0.5)	0.5048(0.0014)	−0.3993(0.0119)	0.1136(0.0283)	−0.2042(0.0184)	
6	5	1.3(0.5)	0.5015(0.0032)	−0.4240(0.0256)	0.2538(0.1301)	−0.4043(0.1815)	0.0899(0.0808)
8	3	2.1(0.7)	0.5068(0.0018)	−0.2308(0.0104)	−0.2412(0.0150)		
8	4	0.6(0.3)	0.5153(0.0019)	−0.3410(0.0260)	0.0405(0.0629)	−0.1852(0.0390)	
8	5	0.6(0.8)	0.5153(0.0051)	−0.3419(0.1697)	0.0444(0.7500)	−0.1904(0.9672)	0.0021(0.3906)
12	3	3.0(1.0)	0.5239(0.0047)	−0.1923(0.0118)	−0.3019(0.0198)		
12	4	1.1(0.6)	0.5400(0.0038)	−0.3614(0.0376)	0.1063(0.0884)	−0.2671(0.0550)	
12	5	1.0(0.6)	0.5438(0.0039)	−0.2783(0.0726)	−0.2779(0.2977)	0.2457(0.3815)	−0.2165(0.1582)
16	3	4.9(1.4)	0.5308(0.0055)	−0.1881(0.0266)	−0.3057(0.0375)		
16	4	1.8(0.8)	0.5520(0.0039)	−0.4948(0.0663)	0.4387(0.1516)	−0.4762(0.0903)	
16	5	1.9(0.9)	0.5538(0.0050)	−0.4403(0.1324)	0.1801(0.5648)	−0.1283(0.7332)	−0.1457(0.3025)

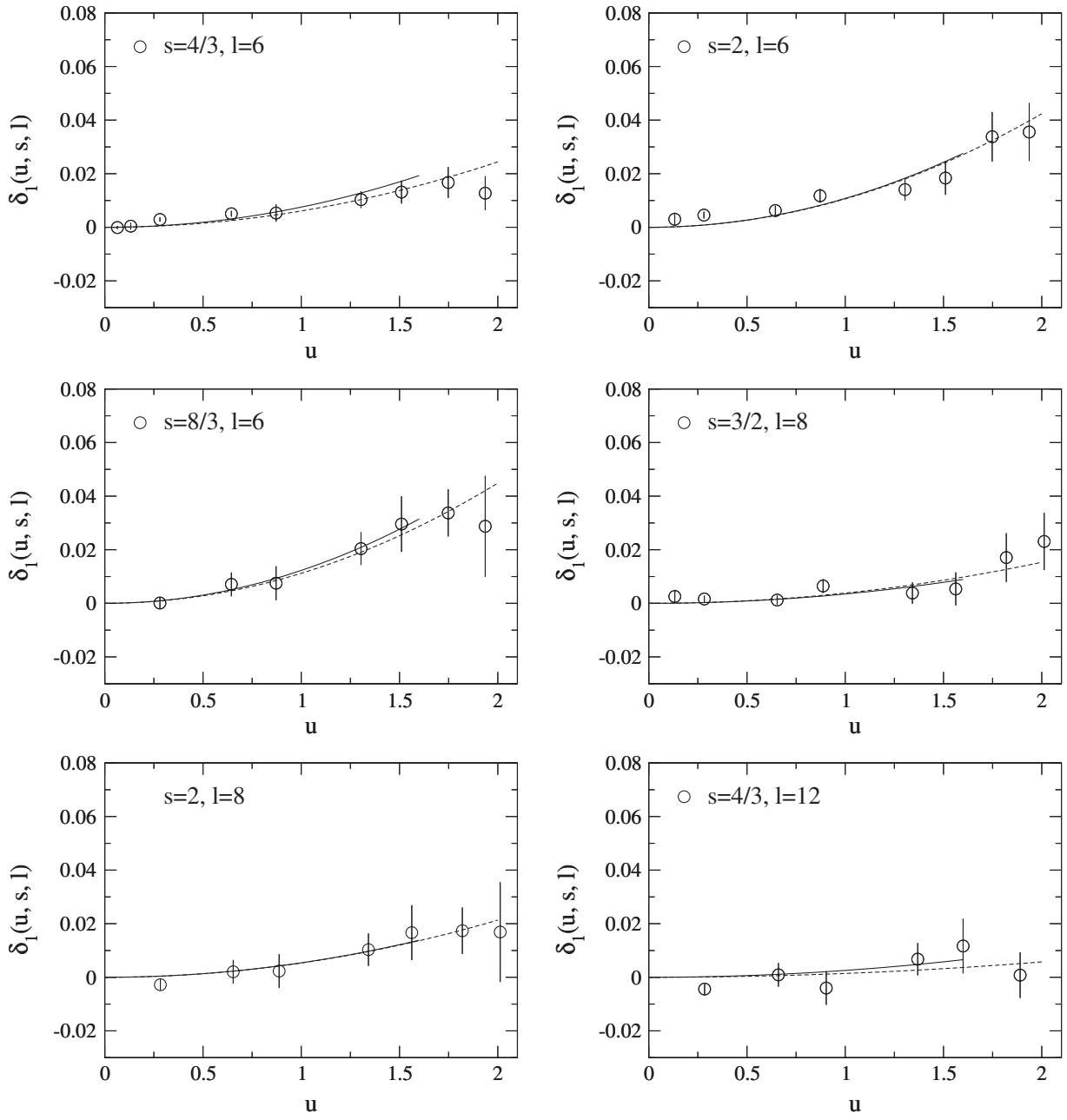

FIG. 2. Fit of δ_1 to a quadratic function of u. The solid and dashed curves show the fit results and the fit ranges.

Since the raw data of $1/g^2_{\rm SF}(g_0^2, l)$ fluctuate around zero in the strong coupling region, converting from $1/g^2_{\rm SF}(g_0^2, l)$ to $g^2_{\rm SF}(g_0^2, l)$ sometimes induces huge statistical uncertainty. To avoid this we treat the inverse coupling constant, $1/g^2_{\rm SF}(g_0^2, l)$, directly. Then, to see the scale dependence of the inverse coupling constant, we introduce the lattice DBF [20,23] by

$$B_0(u, s, l) = \frac{1}{\Sigma_0(u, s, l)} - \frac{1}{u}. \tag{30}$$

We calculate the continuum limit of this function for various initial values of the coupling constant, u. If the sign of the DBF in the continuum limit flips at a certain renormalized coupling constant u, it indicates the existence of IRFP around there.

C. Improving discretization errors

Since $O(a)$ discretization errors are not improved at all in the lattice actions, it is important to remove the scaling violation as much as possible. To do this, we perform the following improvements on the step scaling function and the DBF before taking the continuum limit.

First, let $\sigma(u, s)$ be the continuum limit of $\Sigma_0(u, s, l)$, i.e., $\sigma(u, s) = g^2_{\rm SF}(sL)$ with $u = g^2_{\rm SF}(L)$. Its perturbative expression is given by

TABLE VIII. Coefficients for perturbative correction, $\delta^{(1)}(s, l)$ and $\delta^{(2)}(s, l)$, for each pair of (s, l). The square brackets in the first column indicate the fit range in u.

(s, l)	(4/3, 6)	(2, 6)	(8/3, 6)	(3/2, 8)	(2, 8)	(4/3, 12)
$\delta^{(1)}(s, l)$	−0.001 02	−0.0101	−0.0182	−0.009 05	−0.0172	−0.008 17
$\delta^{(2)}(s, l)$ [0, 1.60]	0.0075(12)	0.0108(15)	0.0123(26)	0.0035(14)	0.0054(24)	0.0026(23)
χ^2/dof	2.2	3.0	0.1	1.0	0.7	1.7
$\delta^{(2)}(s, l)$ [0, 2.0]	0.0061(9)	0.0106(12)	0.0112(18)	0.0038(13)	0.0053(18)	0.0014(17)
χ^2/dof	2.2	2.1	0.2	0.9	0.6	1.4

$$\sigma(u, s) = u + s_0 u^2 + s_1 u^3 + s_2 u^4 + \cdots, \tag{31}$$

$$s_0 = b_1 \ln(s), \tag{32}$$

$$s_1 = \ln(s)(b_1^2 \ln(s) + b_2), \tag{33}$$

$$s_2 = \ln(s)(b_1^3 \ln^2(s) + \frac{5}{2} b_1 b_2 \ln(s) + b_3), \tag{34}$$

where b_i's are the coefficients of the β function introduced in Sec. III. Recalling the parametric form of the discretization error [35], the error normalized by $\sigma(u, s)$, denoted by $\delta_0(u, s, l)$, is written as

$$\delta_0(u, s, l) = \frac{\Sigma_0(u, s, l) - \sigma(u, s)}{\sigma(u, s)} = \delta^{(1)}(s, l)u + \delta^{(2)}(s, l)u^2 + O(u^3). \tag{35}$$

With Eq. (31), the discretization error at the lowest order in u is found to be

$$\delta^{(1)}(s, l) = (p_{1,s\cdot l} - b_1 \ln(s \cdot l)) - (p_{1,l} - b_1 \ln(l)) = p_{1,s\cdot l} - p_{1,l} - b_1 \ln(s). \tag{36}$$

Now by replacing $\Sigma_0(u, s, l)$ in Eq. (35) with $\Sigma_1(u, s, l) = \Sigma_0(u, s, l)/(1 + \delta^{(1)}(s, l)u)$, the discretization error reduces to $O(u^2)$. Using $\Sigma_1(u, s, l)$, the one-loop improved DBF is defined by

$$B_1(u, s, l) = \frac{1}{\Sigma_1(u, s, l)} - \frac{1}{u}. \tag{37}$$

This completes the one-loop improvement.

The above procedure can be repeated to an arbitrarily higher order in u, but it requires the perturbative coefficients like $p_{1,l}$ and the perturbative expression of $\sigma(u, s)$ to the corresponding order in u. All the coefficients necessary for the two-loop improvement are not available at this moment. Instead, we follow an alternative prescription proposed in Ref. [38]. After the one-loop improvement, the scaling violation is written as

$$\delta_1(u, s, l) = \frac{\Sigma_1(u, s, l) - \sigma(u, s)}{\sigma(u, s)} = \delta^{(2)}(s, l)u^2 + O(u^3). \tag{38}$$

If one can somehow know $\delta^{(2)}(s, l)$, the scaling violation can be reduced to $O(u^3)$ by replacing $\Sigma_0(u, s, l)$ in Eq. (35) with

$$\Sigma_2(u, s, l) = \Sigma_0(u, s, l)/(1 + \delta^{(1)}(s, l)u + \delta^{(2)}(s, l)u^2). \tag{39}$$

$\delta^{(2)}(s, l)$ can be determined by fitting our data for $\delta_1(u, s, l)$ in Eq. (38) to the function quadratic in u. Notice that in order for this fitting to make sense, the perturbative series of $\sigma(u, s)$ must be known through $O(u^3)$. Since the first two coefficients, b_1 and b_2, are available, the correct value of $\sigma(u, s)$ can be calculated to $O(u^3)$ as seen from Eq. (31).

$\delta_1(u, s, l)$ is fitted to the form of Eq. (38), neglecting $O(u^3)$ or higher order terms, for all possible pairs of (s, l) as shown in Fig. 2. The fit has to be performed in a weak coupling region where the perturbative expansion is reliable. We examine two fit ranges, $0 \le u \le 1.6$ and $0 \le u \le 2.0$, to see the fit range dependence. The extracted values for $\delta^{(2)}(s, l)$ are tabulated in Table VIII together with $\delta^{(1)}(s, l)$ defined in Eq. (36).

The Table shows that the values of $\delta^{(1)}(s, l)$ and $\delta^{(2)}(s, l)$ lie between 10^{-2} and 10^{-3}, and $\delta^{(2)}(s, l)$ turns out not to depend on the fit range. In the following analysis, we employ $\delta^{(2)}(s, l)$ from the shorter fit range. It is also seen from the Table that generally the coefficients for $(s, l) = (4/3, 12)$ are the smallest among others. This is anticipated because the improvement coefficient vanish as s approaches to unity or l becomes large. An exception is the one-loop coefficient $\delta^{(1)}(4/3, 6)$. Since two-loop coefficient $\delta^{(2)}(4/3, 6)$ is, however, much larger than $\delta^{(1)}(4/3, 6)$, the smallness of $\delta^{(1)}(4/3, 6)$ is probably by accident. In the data sets we have, the data with $(s, l) = (4/3, 6)$ is the coarsest one. As we will show in the following subsections, this data turns out to suffer from nonlinear scaling violation larger than the linear one in the strong coupling region. Thus, we omit this data point throughout the analysis. Using $\delta^{(2)}(s, l)$ thus obtained, we define the two-loop improved step scaling function $\Sigma_2(u, s, l)$ in Eq. (39), and in turn the two-loop improved DBF,

$$B_2(u, s, l) = \frac{1}{\Sigma_2(u, s, l)} - \frac{1}{u}. \tag{40}$$

D. Strategy

The continuum limit is taken for a fixed rescaling factor s and a fixed input length scale L varying a lattice spacing a

$(= L/l)$. As described in the preceding subsections, an input length scale is fixed by choosing a particular value of input coupling u. However, for a given s the number of data sets with different a in this work is, at most, two; $(s, l) = (2, 6)$ and (2,8) for $s = 2$. While it is still possible to employ these two sets of data to evaluate the continuum limit, the validity of the linear extrapolation can not be tested. Alternatively, we may supplement a data set with a desired s by interpolating or extrapolating data of $g^2_{\rm SF}(g_0^2, l)$ in l. However, a lack of guiding principles in the interpolation or extrapolation may cause a systematic uncertainty. In this work, we use the two available data sets, $(s, l) = (2, 6)$ and (2,8), to evaluate the continuum limit by linear extrapolation, and the other data sets are used to monitor the validity of the linear extrapolation. For this purpose, we introduce a relation which approximately converts the DBF for s' into that for s, as follows.

We start with a closer look at the discretization error. The discretization error of the lattice DBF, i.e. $B_i(u, s, l) - B(u, s)$ $(i = 0, 1, 2)$, can be expressed in terms of an asymptotic expansion in $1/l$ [35] as

$$B_i(u, s, l) - B(u, s) = \left(\frac{1}{l} - \frac{1}{sl}\right) e_i(u) + O(l^{-2}), \tag{41}$$

where $e_i(u)$ is an unknown coefficient of $O(a)$ error and is a function of u. We then define the *rescaled* lattice DBF by

$$B'_i(u, s, l, s') = \frac{\ln(s)}{\ln(s')} B_i(u, s', l). \tag{42}$$

In addition, using the continuum counterpart of Eq. (42), we define

$$\delta B(u, s, s') = B(u, s) - \frac{\ln(s)}{\ln(s')} B(u, s'), \tag{43}$$

which represents the difference between the true continuum DBF and the *rescaled* continuum DBF. Combining Eqs. (41)–(43) together and introducing

$$\xi(s, l, s') = \frac{\ln(s)}{\ln(s')}\left(\frac{1}{l} - \frac{1}{s'l}\right), \tag{44}$$

we arrive at

$$B'_i(u, s, l, s') = B(u, s) + \xi(s, l, s') e_i(u) - \delta B(u, s, s') + O(l^{-2}). \tag{45}$$

Therefore, if $\delta B(u, s, s')$ and $O(l^{-2})$ (or higher order) discretization errors are negligible compared to the statistical error of $B'_i(u, s, l, s')$, the numerical data of $B'_i(u, s, l, s')$ plotted against ξ will line up on a single line, and even two unknown coefficients in Eq. (45), $B(u, s)$ and $e_i(u)$, for given u and s can be extracted from that behavior. Instead, if both or one of them is large, the data will not align. Thus, whether $B'_i(u, s, l, s')$ plotted against ξ aligns or not tests the validity of the linear extrapolation within the statistical uncertainty.

We comment on the size of $\delta B(u, s, s')$. Solving Eq. (1) perturbatively, the continuum DBF is found to be

$$B(u, s) = -\ln(s)\left\{\frac{\beta(u)}{u^2} + u^2 \ln(s)\frac{1}{2} b_1 b_2 + u^3 \ln(s) \times \left(\frac{1}{3} b_1^2 b_2 \ln(s) + b_1 b_3 + \frac{1}{2} b_2^2\right)\right\} + O(u^4 \ln^2(s)), \tag{46}$$

and thus the perturbative expression of $\delta B(u, s, s')$ is

$$\delta B(u, s, s') = u^2 \ln(s) \ln\left(\frac{s}{s'}\right)\left[-\frac{1}{2} b_1 b_2 + u\left\{-\frac{1}{3} b_1^2 b_2 \ln(ss') - \left(b_1 b_3 + \frac{1}{2} b_2^2\right)\right\}\right] + O(u^4 \ln(s) \ln(s/s')). \tag{47}$$

Since the numerical values of b_i's are small, e.g. $b_1 \sim 0.055$, $b_2 \sim -0.002$, $b_3^{\rm SF} \sim O(10^{-4})$, $\delta B(u, s, s')$ is also small in the perturbative regime as $10^{-5} \times u^2(1.5 + 0.6u)$, $10^{-5} \times u^2(1.1 + 0.4u)$, and $10^{-5} \times u^2(-1.1 - 0.5u)$ for $(s, s') = (2, 16/12)$, $(2, 12/8)$, and $(s, s') = (2, 16/6)$, respectively. As u becomes large, $\delta B(u, s, s')$ may become sizable and at some point exceed the statistical error of $B'_i(u, s, l, s')$. Then, the alignment will be deformed. Notice that, the smaller $B(u, s')$ is, the smaller $\delta B(u, s, s')$ is, and in particular, when $B(u, s') = 0$ for a certain s', $\delta B(u, s, s') = 0$ holds exactly.

We extract the continuum DBF $B(u, s)$ as follows. First, we assume linear scaling violation and calculate $B(u, s)$ for $s = 2$ by extrapolating the two data sets, $(s', l) = (2, 6)$ and $(2, 8)$, to $\xi = 0$. Since $s' = s$, $B'_i(u, s, l, s') = B_i(u, s', l)$ and $\delta B(u, s, s') = 0$ by construction. Thus, we do not have to rely on the smallness of $\delta B(u, s, s')$. Then, to test the linearity of the scaling violation, we calculate the rescaled lattice DBF $B'_i(u, s, l, s')$ with $s = 2$ from the other data sets and plot them as a function of $\xi(s, l, s')$. If the data align within the statistical error of $B'_i(u, 2, l, s')$, the assumption of the linear scaling violation is valid, $\delta B(u, s, s')$ is negligible, and then the value of $B(u, s)$ thus obtained is reliable. Alternatively, once the linearity is confirmed, we can even determine the continuum limit by taking the linear extrapolation of $B'_i(u, 2, l, s')$. Since $\delta B(u, s, s')$ is negligible in the perturbative regime, the linearity can be tested more rigorously in such a regime. When the data do not align, either or both of the linear violation dominance and small $\delta B(u, s, s')$ are invalid and the result for $B(u, s)$ becomes uncertain.

E. Extraction of the continuum DBF

Extrapolation to the continuum limit described in the following is carried out for every jackknife ensemble, and the statistical error in the continuum limit is estimated by the single elimination jackknife method.

We begin with analysis at relatively weak coupling. Figure 3 shows the continuum limit of $B'_i(u, s, l, s')$ for $s = 2$ $(i = 1, 2)$ at the four representative values of $1/u$ corresponding to $u = 1.0, 2.0, 10/3, 5.0$, where the data

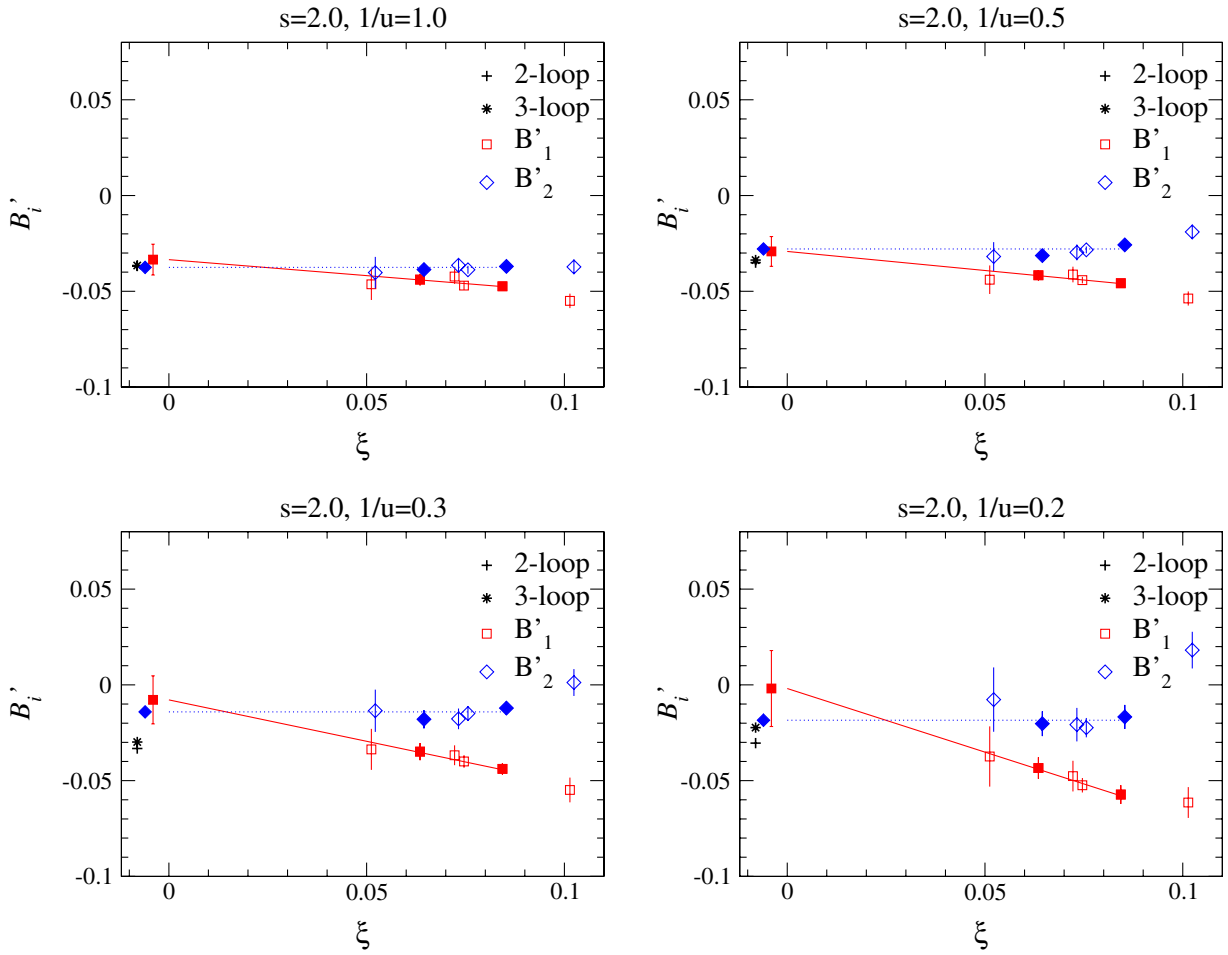

FIG. 3 (color online). Linear extrapolation of B_1 (filled squares) and constant fit of B_2' (filled diamonds) to the continuum limit. The extrapolation and fit use the data with $s' = 2$ (filled symbols). The data with $s' \neq 2$ (open symbols) are also shown to see whether they align or not. The values of (s', l) of the data shown are $(4/3, 6)$, $(2, 6)$, $(8/3, 6)$, $(3/2, 8)$, $(2, 8)$, and $(4/3, 12)$ from right to left. The data points are slightly shifted in the horizontal direction for clarity. The perturbative predictions including the two-loop (plus) and three-loop (star) effects are also shown.

with $s' = 2$ are shown in filled symbols and the other in open symbols and two data of the one-loop improved lattice DBF (B_1') with $s' = 2$ (filled squares) are linearly extrapolated to $\xi = 0$. The two-loop improvement described in Sec. V C is equivalent to tuning the improvement coefficients such that the resulting DBF reproduces the perturbative DBF in the region $0 < u < 1.6$. Indeed, the constant fit of the two-loop improved DBF with $s' = 2$ (filled diamonds) gives the value consistent with the perturbative prediction when $1/u = 1.0$ and 0.5 as seen in the figure. In the same region ($1/u \gtrsim 0.5$), the data of the one-loop improved DBF align and the linear extrapolation reproduces the perturbative DBF as well. Importantly, the extracted continuum DBF is clearly negative in this region.

The deviation from the perturbative prediction appears at $1/u = 0.3$, where the linear extrapolation gives the value closer to and consistent with zero. It is important to note that the data of the one-loop improved DBF align down to $1/u = 0.2$ with a slope increasing with u. From this observation, we conclude that, in the region $1/u \geq 0.2$ ($u \leq 5$), $\delta B(u, s, s')$ is small, the scaling violation is linear for the one-loop improved DBF, and hence the extracted continuum limit is reliable.

Next let us move on to the result at a stronger coupling shown in Fig. 4. As seen from the figure, first the data of B_1' except for the one with $(s', l) = (4/3, 6)$ (rightmost point) remains to align within the statistical uncertainty. Thus, the linear extrapolation of B_1 is reliable at $1/u = 0.15$. Second, the linear extrapolation of B_1 and the constant fit of B_2 lead to different continuum DBF. It appears that the constant fit of B_2 is no longer valid and the linear fit appears to be more reasonable. Indeed, the linear fit of B_2 (solid line and open diamond at $\xi = 0$) turns out to give the consistent limit as shown in the figure.

From the alignment of B_1', we infer that both δB and nonlinear scaling violation remain small. This is consistent with the fact that the continuum DBF obtained by linear

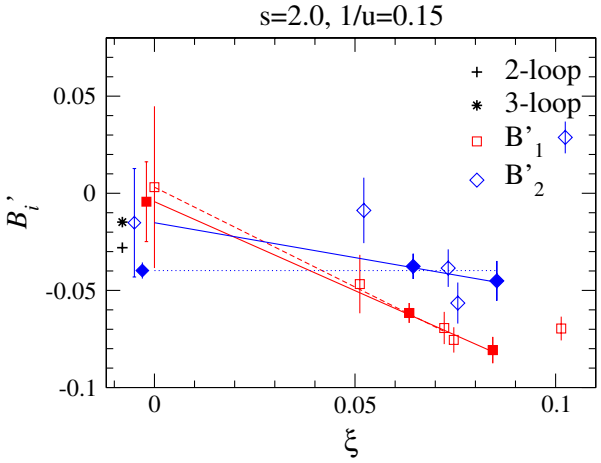

FIG. 4 (color online). Same as Fig. 3, but the result at the stronger coupling is plotted. Solid lines denote the linear extrapolation using the data with $s' = 2$ (filled symbols). The dashed line shows the linear extrapolation using the data with the three smallest ξ.

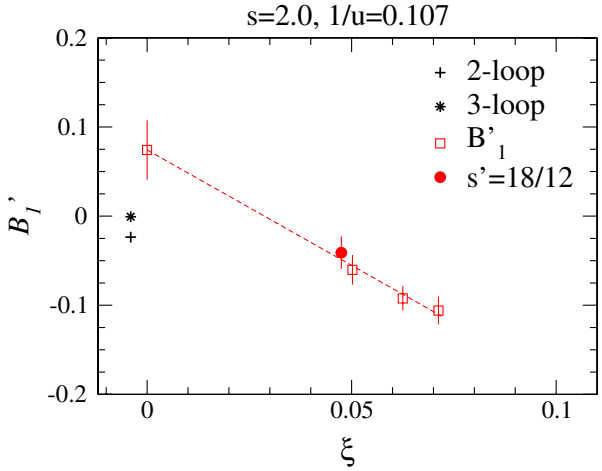

FIG. 5 (color online). Same as Fig. 4 but the data point obtained with $(s', l) = (3/2, 12)$ (filled circle) is included in the analysis at $1/u = 0.107$. The dashed line and the open square at $\xi = 0$ are the result of the linear fit.

extrapolation of B_1 is consistent with zero and thus δB should be small as well.

The deviation of the coarsest data from the linear behavior indicates that the linear discretization error no longer dominates others in the data with $(s', l) = (4/3, 6)$. Since in general nonlinear scaling violation can be large for small l, the data with $l = 6$ may suffer from this though it is not visible in the figure. To evaluate the potential uncertainty due to the $O(l^{-2})$ discretization error, we performed a linear fit without the $l = 6$ data. The fit result is shown as an open square at $\xi = 0$ and the dashed line in Fig. 4. The result is consistent with that using the $s' = 2$ data only.

From Figs. 3 and 4, it turns out that for $1/u \lesssim 0.3$ the extracted continuum DBF is consistent with zero. This indicates that in this region the running coupling constant reaches an infrared fixed point or, at least, the running appreciably slows down. In order to further investigate the existence of the infrared fixed point, we include the data obtained from $l = 18$ lattice at $\beta = 4.55$ into analysis. This data is combined with the data with $l = 12$ to construct B_1' with $(s', l) = (3/2, 12)$. At $\beta = 4.55$, the inverse SF coupling for $l = 12$ turns out to be $1/u = 0.107$. On the $l = 6$ lattice, this value of $1/u$ is realized at $\beta \sim 4.4$. In such a small β, the SF couplings are not calculated on $l = 12, 16$ lattices, and hence the following analysis is carried out without the data from $l = 6$ lattices.

B_1' constructed from the $l = 18$ data is shown in Fig. 5 (filled circle). Since the four data points shown align well, we take the linear extrapolation using all of them and obtain the positive value in $\xi = 0$. Interpretation of this result needs care as mentioned in Sec. II. The most plausible explanation for this observation is that an IRFP exists in $u_{\mathrm{IRFP}} < 1.0/0.107 = 9.35$.

Figure 6 shows the $1/u$ dependence of the continuum DBF, where the results are compared with the perturbative

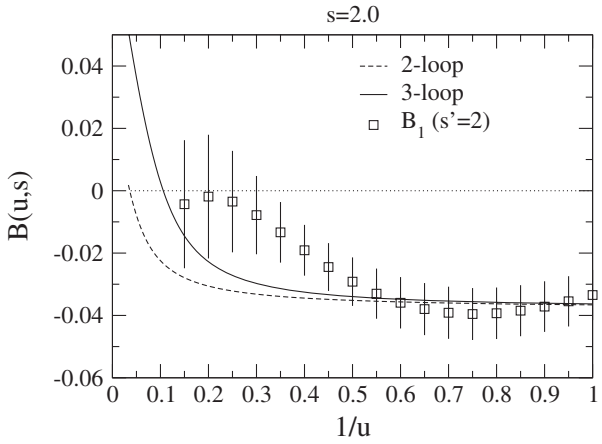

FIG. 6. $1/u$ dependence of $B(u, s)$ with $s = 2$ obtained from the linear extrapolation of the data with $s' = 2$. Two- and three-loop perturbative predictions are shown by the dashed and the solid line, respectively.

calculations. It is seen that the running starts to slow down at around $1/u \sim 0.5$, and eventually the coupling constant reaches a fixed point in the range of $0.107 < 1/u \lesssim 0.3$. When the DBF is positive, it is nontrivial for the continuum limit to exist. Thus, we omit the positive DBF data from the figure.

VI. SUMMARY AND OUTLOOK

In this work, the running coupling constant of ten-flavor QCD is numerically investigated using the lattice technique. The extrapolation of the DBF to the continuum limit is taken linearly assuming that the $O(a)$ scaling violation dominates the higher order ones. The DBF extrapolated approaches zero from below as the SF coupling constant u increases and when $u \gtrsim 10/3$ the DBF becomes consistent

with zero. Further investigation at one particular strong coupling $u = 9.3$ $(1/u = 0.107)$ is made using the data from the large lattice ($l = 18$), and suggests that the continuum DBF at this coupling is not negative. This indicates the existence of the infrared fixed point $10/3 \lesssim g^2_{\mathrm{IRFP}} \lesssim 9.3$. The linear extrapolation is reasonably justified within the statistical error, but further rigorous check is clearly preferable. Combining our result with that of Ref. [12], the critical number of flavors which separates the conformal phase and the broken phase is $8 < N_f^{\mathrm{crit}} < 10$.

In order to confirm the existence of IRFP or even determine the value of the fixed point more precisely, data from larger lattices with high statistics are necessary. It is, however, difficult to do with machines currently available to us, and probably more efficient methods or different approaches are necessary to go further. As mentioned in Sec. I, the conformal window can also be studied by looking at hadrons' spectroscopy or renormalization group analysis on the lattice. Currently the conclusions based on various methods are not consistent among them. In order to pin down N_f^{crit}, these contradictions must be clarified with further studies.

What is really important in the context of the WTC is the anomalous dimension of the $\bar{\psi}\psi$ operator. The calculation of the anomalous dimension in ten-flavor QCD is on-going. The result will be published elsewhere.

Once one has fixed an attractive candidate for WTC, the next important step would be the calculation of the S parameter. The calculational method has been established in Ref. [39], where the QCD S parameter is calculated on the lattice for the first time and is correctly reproduced. Later, the method was applied to three-flavor QCD [40], sextet QCD [41], and six-flavor QCD [42]. In Ref. [42], the evidence of the reduction of the S parameter is reported. Another important quantity which should be calculated is obviously the mass spectrum of the candidate theory, including vector and scalar resonances, the decay constant of the Nambu Goldstone boson, and the chiral condensate. Although the precise determinations of these quantities are challenging, the direct comparison with the upcoming LHC results is extremely interesting and, hence, we believe that such calculations are worth a lot of effort.

ACKNOWLEDGMENTS

N. Y. thanks the Aspen Center for Physics where the workshop ''Strong Coupling Beyond the Standard Model'' were held during May and June 2010 and the Yukawa Institute for Theoretical Physics at Kyoto University for supporting the YITP workshop ''Summer Institute 2010'' (YITP-W-10-07). A part of this work was completed during these workshops. N. Y. would also like to thank Hideo Matsufuru, Yoshio Kikukawa, and Takashi Kaneko for useful discussion. The main part of the numerical simulations were performed on Hitachi SR11000 and the IBM System Blue Gene Solution at High Energy Accelerator Research Organization (KEK) under the support of its Large Scale Simulation Program (No. 09/10-01, 10-15), on the B-factory computer system at KEK, on the GCOE (Quest for Fundamental Principles in the Universe) cluster system at Nagoya University, and on the INSAM (Institute for Numerical Simulations and Applied Mathematics) GPU cluster at Hiroshima University. This work is supported in part by the Grant-in-Aid for Scientific Research of the Japanese Ministry of Education, Culture, Sports, Science and Technology and JSPS (No. 20105001, No. 20105002, No. 20105005, No. 21684013, No. 22740183, No. 22011012, No. 20540261, No. 22224003, No. 20740139, No. 18104005, No. 22244018, and No. 227180), and by U.S. DOE Grant No. DE-FG02-92ER40699.

[1] S. Weinberg, Phys. Rev. D **13**, 974 (1976); L. Susskind, Phys. Rev. D **20**, 2619 (1979).
[2] E. Eichten and K. D. Lane, Phys. Lett. **90B**, 125 (1980); S. Dimopoulos and L. Susskind, Nucl. Phys. **B155**, 237 (1979).
[3] R. S. Chivukula, arXiv:hep-ph/0011264; C. T. Hill and E. H. Simmons, Phys. Rep. **381**, 235 (2003); **390**, 553 (E) (2004); F. Sannino, arXiv:0804.0182.
[4] M. E. Peskin and T. Takeuchi, Phys. Rev. Lett. **65**, 964 (1990); Phys. Rev. D **46**, 381 (1992).
[5] See, for example, R. S. Chivukula and E. H. Simmons, Phys. Rev. D **82**, 033014 (2010).
[6] B. Holdom, Phys. Rev. D **24**, 1441 (1981); K. Yamawaki, M. Bando, and K. i. Matumoto, Phys. Rev. Lett. **56**, 1335 (1986); T. W. Appelquist, D. Karabali, and L. C. R. Wijewardhana, Phys. Rev. Lett. **57**, 957 (1986); T. Akiba and T. Yanagida, Phys. Lett. **169B**, 432 (1986); M. Bando, T. Morozumi, H. So, and K. Yamawaki, Phys. Rev. Lett. **59**, 389 (1987).
[7] D. D. Dietrich and F. Sannino, Phys. Rev. D **75**, 085018 (2007).
[8] W. E. Caswell, Phys. Rev. Lett. **33**, 244 (1974); T. Banks and A. Zaks, Nucl. Phys. **B196**, 189 (1982).
[9] For a recent review, see, for example, G. T. Fleming, Proc. Sci. , LAT2008 (2008) 021 [arXiv:0812.2035]; E. Pallante, Proc. Sci. LAT2009 (2009) 015 [arXiv:0912.5188].
[10] H. Gies and J. Jaeckel, Eur. Phys. J. C **46**, 433 (2006).
[11] J. Braun and H. Gies, J. High Energy Phys. 06 (2006) 024.
[12] T. Appelquist, G. T. Fleming, and E. T. Neil, Phys. Rev. Lett. **100**, 171607 (2008); arXiv:0712.0609.

[13] T. Appelquist, G. T. Fleming, and E. T. Neil, Phys. Rev. D **79**, 076010 (2009).
[14] A. Deuzeman, M. P. Lombardo, and E. Pallante, Phys. Lett. B **670**, 41 (2008).
[15] A. Deuzeman, M. P. Lombardo, and E. Pallante, Phys. Rev. D **82**, 074503 (2010).
[16] Z. Fodor, K. Holland, J. Kuti, D. Nogradi, and C. Schroeder, Phys. Lett. B **681**, 353 (2009).
[17] A. Hasenfratz, Phys. Rev. D **80**, 034505 (2009).
[18] X. Y. Jin and R. D. Mawhinney, Proc. Sci. LAT2009 (2009) 049 [arXiv:0910.3216].
[19] E. Bilgici *et al.*, Proc. Sci. LAT2009 (2009) 063 [arXiv:0910.4196].
[20] Y. Shamir, B. Svetitsky, and T. DeGrand, Phys. Rev. D **78**, 031502 (2008).
[21] T. DeGrand, Y. Shamir, and B. Svetitsky, Phys. Rev. D **79**, 034501 (2009).
[22] T. DeGrand, Phys. Rev. D **80**, 114507 (2009).
[23] T. DeGrand, Y. Shamir, and B. Svetitsky, Phys. Rev. D **82**, 054503 (2010).
[24] Z. Fodor, K. Holland, J. Kuti, D. Nogradi, and C. Schroeder, J. High Energy Phys. 11 (2009) 103.
[25] J. B. Kogut and D. K. Sinclair, Phys. Rev. D **81**, 114507 (2010).
[26] A. J. Hietanen, K. Rummukainen, and K. Tuominen, Phys. Rev. D **80**, 094504 (2009).
[27] A. J. Hietanen, J. Rantaharju, K. Rummukainen, and K. Tuominen, J. High Energy Phys. 05 (2009) 025.
[28] L. Del Debbio, B. Lucini, A. Patella, C. Pica, and A. Rago, Phys. Rev. D **80**, 074507 (2009).
[29] F. Bursa, L. Del Debbio, L. Keegan, C. Pica, and T. Pickup, Phys. Rev. D **81**, 014505 (2010).
[30] L. Del Debbio, B. Lucini, A. Patella, C. Pica, and A. Rago, Phys. Rev. D **82**, 014509 (2010).
[31] L. Del Debbio, B. Lucini, A. Patella, C. Pica, and A. Rago, Phys. Rev. D **82**, 014510 (2010).
[32] M. Luscher, R. Narayanan, P. Weisz, and U. Wolff, Nucl. Phys. **B384**, 168 (1992); M. Luscher, R. Sommer, P. Weisz, and U. Wolff, Nucl. Phys. **B413**, 481 (1994); S. Sint and R. Sommer, Nucl. Phys. **B465**, 71 (1996).
[33] S. Aoki *et al.* (JLQCD Collaboration), Phys. Rev. D **72**, 054510 (2005).
[34] K. i. Nagai, G. Carrillo-Ruiz, G. Koleva, and R. Lewis, Phys. Rev. D **80**, 074508 (2009).
[35] A. Bode, P. Weisz, and U. Wolff (ALPHA collaboration), Nucl. Phys. **B576**, 517 (2000); **B600**, 453(E) (2001); **B608**, 481(E) (2001).
[36] T. Appelquist, K. D. Lane, and U. Mahanta, Phys. Rev. Lett. **61**, 1553 (1988); A. G. Cohen and H. Georgi, Nucl. Phys. **B314**, 7 (1989).
[37] M. Hayakawa, K.-I. Ishikawa, Y. Osaki, S. Takeda, S. Uno, and N. Yamada, Proc. Sci. LATTICE2010 (2010) 325 [arXiv:1009.5169].
[38] S. Aoki *et al.* (PACS-CS Collaboration), J. High Energy Phys. 10 (2009) 053.
[39] E. Shintani *et al.* (JLQCD Collaboration), Phys. Rev. Lett. **101**, 242001 (2008).
[40] P. A. Boyle, L. Del Debbio, J. Wennekers, and J. M. Zanotti (RBC Collaborations and UKQCD Collaborations), Phys. Rev. D **81**, 014504 (2010).
[41] T. DeGrand, arXiv:1006.3777.
[42] T. Appelquist *et al.*, arXiv:1009.5967 [Phys. Rev. Lett. (to be published)].